frontiers in Chemistry

ORIGINAL RESEARCH
published: 15 March 2021
doi: 10.3389/fchem.2021.638581

Comparison Between Electride Characteristics of $Li_3@B_{40}$ and $Li_3@C_{60}$

Prasenjit Das[1] *and Pratim Kumar Chattaraj*[1,2]*

[1]Department of Chemistry, Indian Institute of Technology Kharagpur, Kharagpur, India, [2]Department of Chemistry, Indian Institute of Technology Bombay, Mumbai, India

Density functional theory (DFT) based computation is performed on the endohedrally encapsulated Li_3 cluster inside the B_{40} and C_{60} cages namely, $Li_3@B_{40}$ and $Li_3@C_{60}$. For both these systems, the Li-Li bond lengths are shorter than that in the free Li_3 cluster. Due to confinement, the Li-Li vibrational frequencies increase in both the systems as compared to that in the free Li_3 cluster. Thermodynamically, the formation of these two systems is spontaneous in nature as predicted by the negative values of Gibbs' free energy changes (ΔG). For both the systems one non-nuclear attractor (NNA) is present on the middle of the Li_3 cluster which is predicted and confirmed by the electron density analysis. The NNA population and the percentage localization of electron density at the NNA of the $Li_3@C_{60}$ system are higher than that in the $Li_3@B_{40}$ system. At the NNA the values of the Laplacian of electron density are negative and an electron localization function basin is present at the center of the Li_3 cluster for localized electrons. Both systems show large values of nonlinear optical properties (NLO). Both the Li_3 encapsulated endohedral systems behave as electrides. Electrides have low work function and hence have a great potential in catalytic activity toward the activation of small molecules (such as CO_2, N_2). Even some electrides have greater catalytic activity than some well-studied metal-loaded catalysts. As the systems under study behave as electrides, they have the power to show catalytic activity and can be used in catalyzing the activation of small molecules.

Keywords: endohedral encapsulation, electride, non-nuclear attractor, electron localization function basin, nonlinear optical properties properties

OPEN ACCESS

Edited by:
Sailaja Krishnamurty, National Chemical Laboratory (CSIR), India

Reviewed by:
Lin Zhong, Sichuan University, China
Yang Liu, Dalian University of Technology, China

***Correspondence:**
Pratim Kumar Chattaraj
pkc@chem.iitkgp.ac.in

Specialty section:
This article was submitted to Catalysis and Photocatalysis, a section of the journal Frontiers in Chemistry

Received: *07 December 2020*
Accepted: *02 February 2021*
Published: *15 March 2021*

Citation:
Das P and Chattaraj PK (2021) Comparison Between Electride Characteristics of $Li_3@B_{40}$ and $Li_3@C_{60}$. Front. Chem. 9:638581. doi: 10.3389/fchem.2021.638581

INTRODUCTION

Electrons trapped inside the cavity of some interesting ionic systems behave as anions giving rise to electrides (Dye, 2003; Garcia-Borrà;s et al., 2012; Postils et al., 2015; Zhao et al., 2016; Saha et al., 2019). In recent year's electride properties of materials have generated great attention in experiments as well as in the theoretical studies. The inception of the concept of an electride took place during the study of the solvated electrons in the solution of alkali metal systems in ammonia (Greenlee and Henne, 1946; Zurek et al., 2009). Dye et al., 1970; Dye, 1990; Dye, 1991; Dye, 1997; Dye, 2003) provided valuable studies on electride materials. The trapped electrons are not attached to any particular atom but located at the cavities and the interstices of cryptands and solid crystals, respectively (Zhao et al., 2016; Dale and Johnson, 2018). The electron density analysis confirmed the presence of confined electrons in the cavities of solid alkali metals (Marqués et al., 2009; Mei et al., 1993). Ellaboudy et al. (1983) synthesized the first stable organic electride, $Cs^+(18\text{-crown-}6)_2e^-$ in the crystalline form and Matsuishi et al. (2003) synthesized the first stable inorganic electride, $[Ca_{24}Al_{28}O_{64}]^{4+}\cdot(4e^-)$. In both cases, the excess electrons are confined in the empty area of those

crystals. This is followed by the synthesis and characterization of six temperature and air-stable electride systems (Ward et al., 1988, Ward et al.,1990a; Ward et al., 1990b; Wagner et al., 1994; Huang et al., 1997; Xie et al., 2000; Redko et al., 2005). In these systems, the cryptand ligands or crown ethers are complexed with alkali metals. Electride materials are very sensitive to temperature and air (Sun et al., 2016). So, it becomes a challenging task to generate and characterize electride materials which are stable related to air and temperature. The presence of cavity trapped loose electrons causes a lowering of the work function of electrides so that they can be used as an electron donor in chemical reactions. Moreover, the presence of loose electrons is responsible in making the electride systems very important because of their potential applications for example the emitting diodes for organic light (Yanagi et al., 2009), reversible hydrogen storage materials (Kitano et al., 2012), catalyst for the CO_2 activation (Toda et al., 2013), splitting of N_2 molecule (Kitano et al., 2012, 2015; Lu et al., 2016), powerful reducing agents (Buchammagari et al., 2007; Choi et al., 2014; Kim et al., 2014), and superconductivity (Miyakawa et al., 2007). The experimental identification of the position of localized trapped electrons is very difficult because of the low density of these localized electrons. So, experimentalist used indirect evidence for its experimental characterization (Singh et al., 1993; Dye, 1997). Therefore, computational studies can be helpful for the identification of electride materials. For that purpose, people used different computational tools to characterize electride materials. One can in silico characterize a material to behave as an electride and the necessary conditions for the same are, 1) presence of non-nuclear attractors (NNA) of the electron density (Dye, 2003; Lee et al., 2013; Dale et al., 2014); 2) the Laplacian of electron density ($\nabla^2\rho$) should be negative at the NNAs; 3) existence of electron localization function (ELF) basin at the NNA region; 4) high values of NLO properties. Some molecules which do not possesses confined electrons in electronic structure can show one or more of the above-mentioned properties. Thus, none of these conditions alone can be used to characterize electride systems, unambiguously. Some previous studies reported some molecules as electride material based on large NLOPs are not considered to be materials with electride properties on these days. When all of these four criteria are simultaneously satisfied, we can say that a cavity-trapped electron is present within the structure of a molecule and it constitutes a real electride material. We will analyze all of the above criteria in detail to check whether they present systems qualify to be termed as electrides. Most recently one theoretical work has shown that binuclear sandwich complexes of Be and Mg atoms bonded with isoelectronic $C_5H_5^-$, N_5^-, P_5^-, As_5^- ligands obeyed all these above-mentioned criteria to behave as electride materials (Das and Chattaraj, 2020).

After the discovery of buckminsterfullerene (C_{60}) in 1985, people became interested in using its cavity for the encapsulations of metals, and gas molecules (Kroto et al., 1985). Endohedral fullerenes are very useful in biology (Cagle et al., 1996), in molecular electronics (Jaroš et al., 2019), in nuclear magnetic resonance (NMR) analysis, and in magnetic resonance imaging (Kato et al., 2003). The exterior surface of fullerenes has been used for various chemical reactions to take place (Levitt, 2013). The first experimentally synthesized endohedral fullerene is La@C_{60} (Heath et al., 1985). Experimentally, Hiroshi et al. reported the endohedral encapsulation of Li^+ ion inside the C_{60} cage (Ueno et al., 2015). Experimentally Li, Ca, Pr, Y, Ba, Ce, Nd, Gd metals (Ding and Yang, 1996; Kubozono et al., 1996; Wan et al., 1998; Okada et al., 2012) and He, Ne, Ar, Kr, Xe noble gases (Saunders et al., 1993; Saunders et al., 1994; Ohtsuki et al., 1998) were kept inside the C_{60} cage. Using the "molecular surgery" approach, it is experimentally reported for the endohedral encapsulation of H_2 (Komatsu et al., 2005; Murata et al., 2008), H_2O (Kurotobi and Murata, 2011), HF (Krachmalnicoff et al., 2016), CH_4 (Bloodworth et al., 2019) molecules inside fullerene. Several theoretical works have been reported for the encapsulation of different noble gases and metals inside the C_{60} cage (Andreoni and Curioni, 1996; Bühl et al., 1997; Strenalyuk and Haaland, 2008). Theoretically, Krapp and Frenking have studied the possibility of the encapsulation of noble gas dimers inside the C_{60} cage and showed the formation of noble gas-noble gas (Ng-Ng) 'genuine' chemical bond for Ar, Kr, and Xe, whereas weak interactions are present for He and Ne (Krapp and Frenking, 2007). Theoretically, Khatua et al. (2014a) studied the confinement of HF dimer inside the C_{60}, C_{70}, C_{80}, and C_{90} cages. Using the *ab-initio* molecular dynamics study the movement of Ng_2 dimer inside the C_{60} cage has been reported (Khatua et al., 2014b). Recently, endohedral encapsulation of Mg_2 molecule inside the C_{60} cage and the bonding interactions therein have also been studied (Das et al., 2020).

Borospherene, the boron analogue of fullerene has achieved great attention to the scientist. The first reported borospherene is B_{40} having a cage-like structure (Zhai et al., 2014). After that several borospherenes such as B_{28}, B_{38}, B_{44}, B_{46}, B_{29}^-, B_{37}^-, B_{38}^-, B_{39}^-, B_{44}^-, B_{39}^+, B_{40}^+, B_{41}^+, B_{42}^{2+}, and their various metal doped homologues have been reported experimentally as well as theoretically (Lv et al., 2014; Chen et al., 2015; Zhao et al., 2015; Li et al., 2016a; Li et al., 2016b; Tai and Nguyen, 2016; Tian et al., 2016; Li et al., 2017; Tai and Nguyen, 2017). Pan et al. (2018) studied the endohedral encapsulation of noble gas monomer and dimer inside the B_{40} cage and the bonding interactions between Ng-B and Ng-Ng using density functional theory (DFT). Furthermore, the endohedral encapsulation of noble gas dimer inside the cavitand of cucurbit[6]uril and octa acid has been reported (Pan et al., 2015; Chakraborty et al., 2016). Theoretically, Das and Chattaraj (2014) studied the encapsulation of alkali and alkaline earth metals inside an aza crown analogue, $[(N_4C_2H_2)_4]^{2-}$ and the bonding interactions therein.

In this article we attempt to analyze molecules with electride property and for that purpose, we have encapsulated the Li_3 cluster in two different cages, B_{40} and C_{60} and they are denoted as $Li_3@B_{40}$ and $Li_3@C_{60}$. We have used density functional theory (DFT) for the study of the structure, stability, and nature of bonding in these systems. We have computed the Gibbs' free

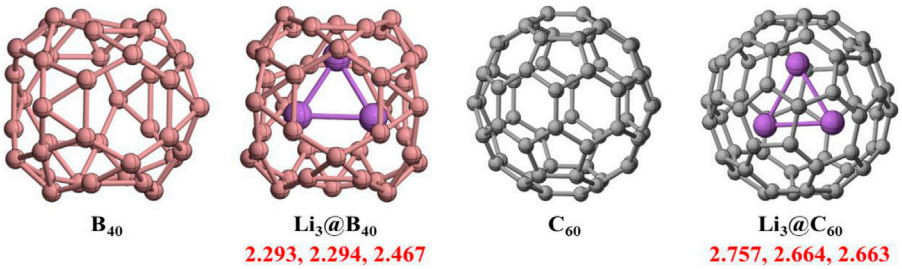

FIGURE 1 | The optimized geometries of B_{40}, C_{60} cages, and $Li_3@B_{40}$ and $Li_3@C_{60}$ systems at BP86-D3/def2-TZVPP method. The values in red color indicate Li-Li bond lengths (r_{Li-Li}). The bond lengths are in the Å unit.

energy change for the formation of both the electride systems in gas phase as well as in toluene and benzene solvent phases. The molecular orbital analysis and the electron density analysis of both these systems have been performed. Then we have calculated and compared the NLO properties of these systems. Finally, the electride characteristics of these two systems have been analyzed and the same between them have been compared.

COMPUTATIONAL DETAILS

We have used BP86-D3/def2-TZVPP method (Perdew, 1986; Becke, 1988; Weigend and Ahlrichs, 2005; Grimme et al., 2010) for geometry optimization and subsequent frequency calculations. The real harmonic frequency values indicate that these are the energy minimum structures on their respective potential energy surfaces. The Gaussian 16 program package has been used for all the computations (Frisch et al., 2016).

The atom centered density matrix propagation (ADMP) simulation has been carried out at BP86/6–31G method to know about the dynamical behavior of our systems at 300 K and 500 K temperatures and 1 atm pressure over 700 fs of time.

We have carried out the natural bond orbital (NBO) analysis to know the charge distribution on each atom. The computation for this analysis has been carried out at BP86-D3/def2-TZVPPD//BP86-D3/def2-TZVPP level of theory using NBO 3.1 version (Reed et al., 1988; Glendening et al., 1990) as implemented in Gaussian 16.

Multiwfn program package (Lu and Chen, 2012) has been used for atoms-in-molecule analysis (AIM) (Bader, 1990) of electron density. We have used BP86-D3/def2-TZVPPD//BP86-D3/def2-TZVPP method for this analysis and various bond critical points (BCP) have been generated. Both AIM and ELF basin population have been analyzed.

For the calculation of the average polarizability ($\bar{\alpha}$), first hyperpolarizability (β), and second hyperpolarizability ($\gamma_{\parallel}$), B3LYP/6-31+G(d)/6-31+G//BP86-D3/def2-TZVPP method has been used, where, 6-31+G(d) basis set is used for Li atoms and 6-31+G basis set is used for C and B atoms.

To compute the $\bar{\alpha}$, β and $\gamma_{\parallel}$ values the following equations have been used (Bishop and Norman, 2001),

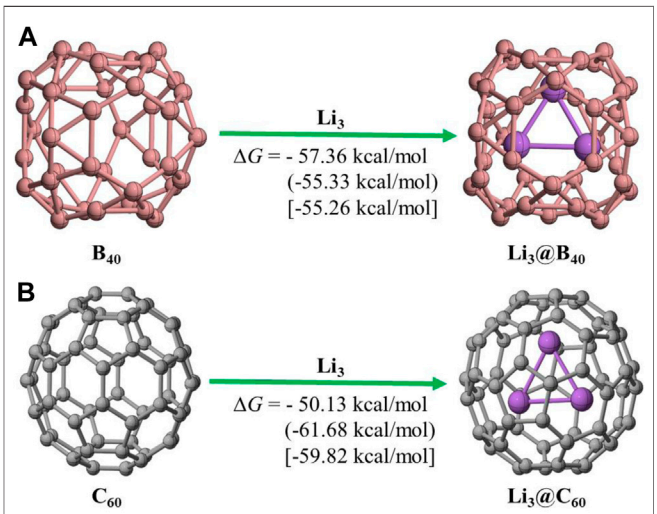

FIGURE 2 | The Schematic representation of the reaction path for **(A)** $Li_3@B_{40}$; **(B)** $Li_3@C_{60}$ systems considered in the study. The values without parentheses are calculated ΔG values at gas phase. The values within parentheses and within square brackets are calculated ΔG values at toluene and benzene solvent phases, respectively.

$$\bar{\alpha} = \frac{1}{3}\sum_{i=x,y,z}\alpha_{ii},$$

$$\beta = \left(\sum_{i=x,y,z}\beta_i^2\right)^{1/2},$$

$$\text{where, } \beta_i = \frac{1}{3}\sum_{j=x,y,z}\left(\beta_{ijj}+\beta_{jij}+\beta_{jji}\right),$$

$$\gamma_{\parallel} = \frac{1}{15}\sum_{i,j=x,y,z}\left(\gamma_{iijj}+\gamma_{ijij}+\gamma_{ijji}\right).$$

RESULTS AND DISCUSSION

Geometries and Energetics

The optimized geometries of B_{40} and C_{60} cages and the $Li_3@B_{40}$ and $Li_3@C_{60}$ systems without any symmetry constraint are given in **Figure 1**. The B_{40} and C_{60} cages have D_{2d} and C_{2h} point groups of

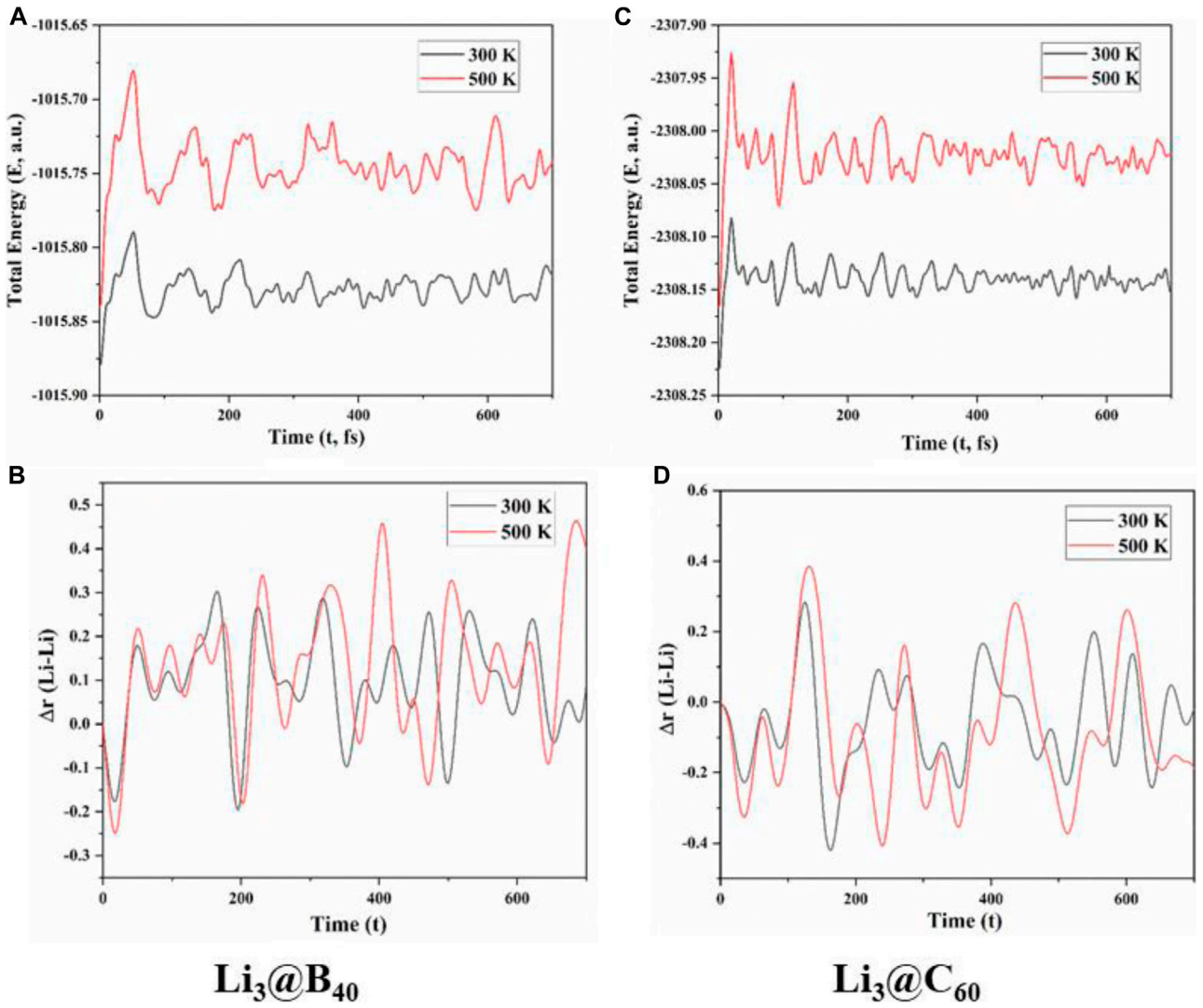

FIGURE 3 | (A) and **(C)** Time evolution of total energy for $Li_3@B_{40}$ and $Li_3@C_{60}$ systems, respectively, **(B)** and **(D)** change in the Li-Li bond lengths with respect to the corresponding optimized value (at t = 0) against time for $Li_3@B_{40}$ and $Li_3@C_{60}$ systems, respectively.

symmetry, respectively, and the $Li_3@B_{40}$ and $Li_3@C_{60}$ systems have C_1 point group of symmetry. The Li-Li bond lengths are 2.293 Å, 2.294 Å, and 2.467 Å for the $Li_3@B_{40}$ system, and for the $Li_3@C_{60}$ system, the Li-Li bond distances are 2.757 Å, 2.663 Å, and 2.664 Å. For both the systems the Li-Li bond lengths are shorter than that in the free Li_3 cluster. The confinement effect of B_{40} and C_{60} cages can account for this short Li-Li bond length for $Li_3@B_{40}$ and $Li_3@C_{60}$ systems, respectively. For the $Li_3@B_{40}$ system, the Li-Li bond lengths are shorter than that in the $Li_3@C_{60}$ systems. This is because of the comparatively smaller size of the B_{40} cage than that of the C_{60} cage. The numerical values of vibrational frequencies of Li-Li bonds for both $Li_3@B_{40}$ and $Li_3@C_{60}$ systems are presented in **Supplementary Table S1**. From the numerical values of Li-Li vibrational frequencies for both the systems, it has been found that there is an increase in the vibrational frequencies as compared to that in the free Li_3 cluster (139.6 cm^{-1}, 185 $cm^{-1,}$ and 301.8 cm^{-1}). $Li_3@B_{40}$ system has higher values of Li-Li vibrational frequency as compared to that of the $Li_3@C_{60}$ systems.

For these endohedral encapsulation processes the Gibbs' free energy changes (ΔG) in gas phase are −57.36 kcal/mol and −50.13 kcal/mol for $Li_3@B_{40}$ and $Li_3@C_{60}$ systems, respectively. For $Li_3@B_{40}$ system the ΔG values are −55.33 kcal/mol and −55.26 kcal/mol in toluene and in benzene solvents, respectively. However, for $Li_3@C_{60}$ system the ΔG values are −61.68 kcal/mol and −59.82 kcal/mol in toluene and in benzene solvents, respectively. The ΔG values are computed at BP86-D3/def2-TZVPP level of theory. The negative values of ΔG as shown in **Figure 2** indicate the spontaneous formation of these endohedral systems in gas phase as well as in the solvents. So, both the hosts, B_{40} and C_{60} cages can hold and stabilize the guest Li_3 cluster inside their cavity.

To know about the dynamical behavior of these systems we have carried out ADMP simulation at BP86/6-31G level of theory

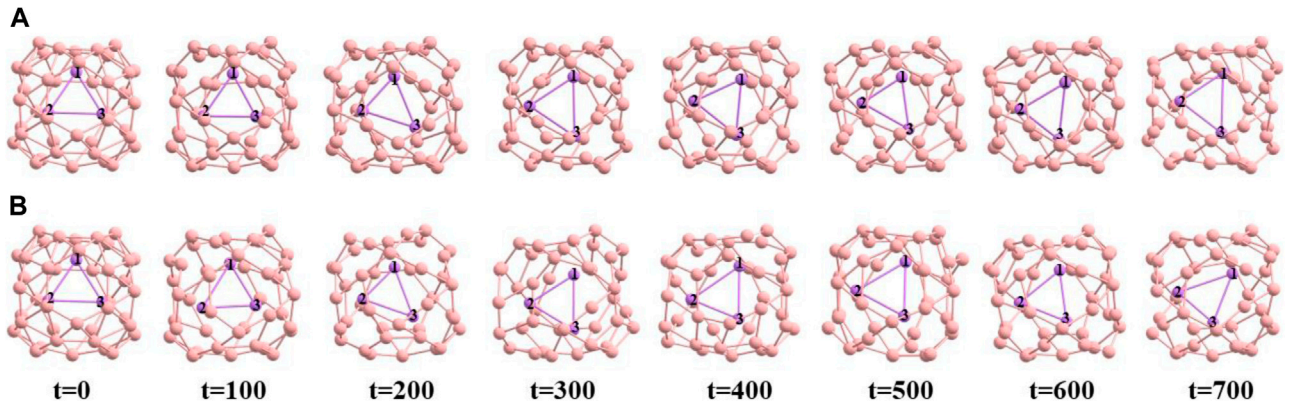

FIGURE 4 | Snapshots at different time steps (time in fs) **(A)** at 300 K temperature, **(B)** at 500 K temperature of $Li_3@B_{40}$ system.

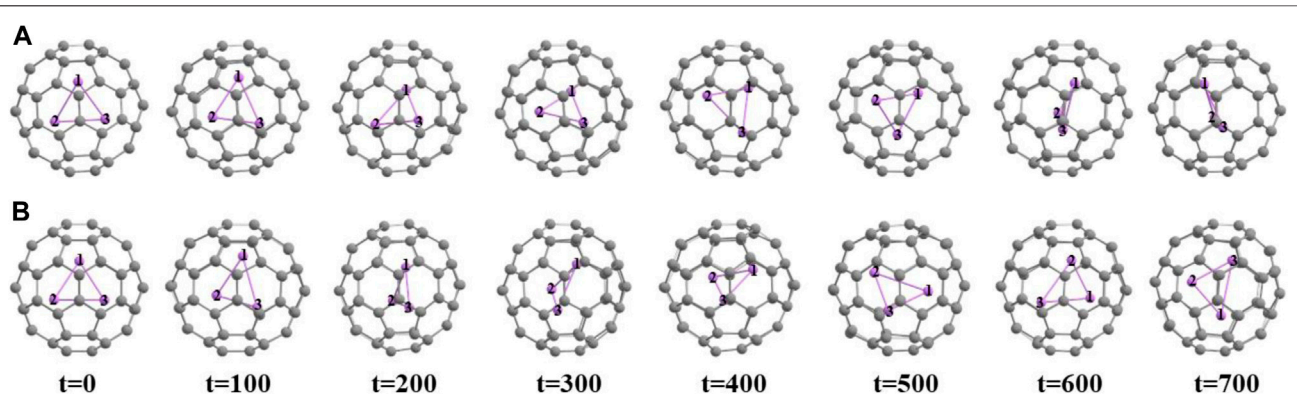

FIGURE 5 | Snapshots at different time steps (time in fs) **(A)** at 300 K temperature, **(B)** at 500 K temperature of $Li_3@C_{60}$ system.

at both 300 K and 500 K temperature and at 1 atm pressure over 700 fs of time. We have presented the time evolution of the energy plots in **Figures 3A**,C for $Li_3@B_{40}$ and $Li_3@C_{60}$ systems, respectively. During structural deformation the nuclear kinetic energy of the systems increases which causes the oscillation in the time evolution of energy plots. From the time evolution plot of Li-Li bond length (**Figures 3B**,D for $Li_3@B_{40}$ and $Li_3@C_{60}$ systems, respectively) it is shown that the Li-Li bond lengths are fluctuating around the corresponding equilibrium values without disintegrating the systems. The different orientations of the Li_3 cluster inside the B_{40} and C_{60} cages at these temperatures at different time steps are shown in **Figures 4**, **5**, respectively. At both temperatures, the Li_3 cluster is only moving inside the cages without breaking the cages. So we can say that these two systems are stable at room temperature as well as at 500 K temperature. So, the guest Li_3 cluster can stay inside the B_{40} and C_{60} cages.

NATURE OF BONDING

Molecular Orbitals

We have used BP86-D3/def2-TZVPP method for molecular orbital analysis of both systems. The highest occupied molecular orbital (HOMO), HOMO-1, and lowest unoccupied molecular orbital (LUMO) for the systems are presented in **Figure 6**. For the $Li_3@B_{40}$ system, the HOMO-1 and LUMO are distributed over the B_{40} cage but there is no contribution from the Li_3 moiety. For the $Li_3@C_{60}$ system, the HOMO and LUMO are π-type of orbitals and are distributed over the C_{60} cage but there is no contribution from the Li_3 moiety. The energy differences between HOMO and LUMO are 0.62 eV and 0.18 eV for $Li_3@B_{40}$ and $Li_3@C_{60}$ systems, respectively. The spin density plots are presented in **Figures 6C,D** for $Li_3@B_{40}$ and $Li_3@C_{60}$ system, respectively. The spin density plots show that the total spin density is distributed over the guest Li_3 cluster and the host B_{40} and C_{60} cages.

Natural Bond Orbital Analysis

The charge distribution over the atoms in both the systems has been analyzed by natural bond orbital analysis. For $Li_3@C_{60}$ system the natural charges on Li atoms are 0.60 $|e|$, 0.60 $|e|$, and 0.55 $|e|$. While the charges on Li atoms are 0.60 $|e|$, 0.73 $|e|$, and 0.74 $|e|$ for $Li_3@B_{40}$ system. The charges on the Li atoms are higher in case of $Li_3@B_{40}$ system as compared to that in the $Li_3@C_{60}$ system. In both the systems charge transfer takes place from the guest Li_3 cluster to the host B_{40} and C_{60} cages. In $Li_3@B_{40}$

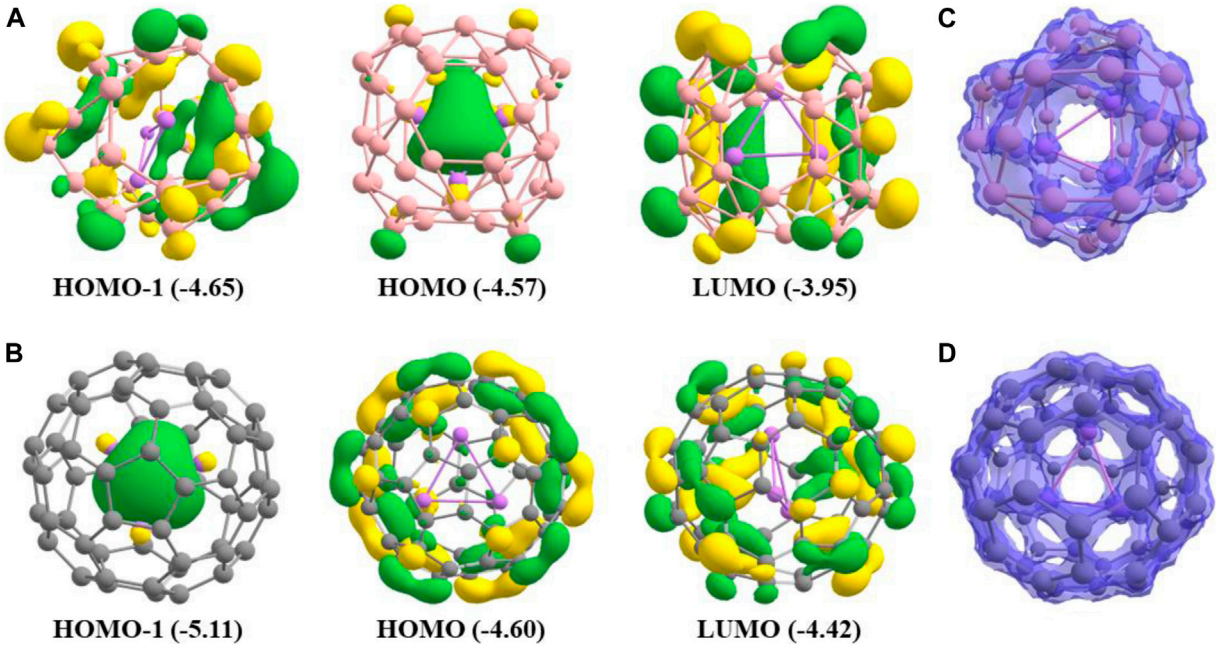

FIGURE 6 | Plots of the HOMO-1, HOMO, and LUMO for **(A)** $Li_3@B_{40}$ system, **(B)** $Li_3@C_{60}$ system, **(C)** and **(D)** are spin density for $Li_3@B_{40}$ and $Li_3@C_{60}$ system, respectively. The values in the parenthesis are the energies of the corresponding orbitals in the eV unit.

TABLE 1 | Electron Density [$\rho(r_c)$], Laplacian of Electron Density [$\nabla^2\rho(r_c)$], Kinetic Energy Density [$G(r_c)$], Potential Energy Density [$V(r_c)$], Total Energy Density [$H(r_c)$], Basin Population [N(pop)], Localization Index (LI), Percentage of Localization Index (% LI) at Different Critical Points (CP) of the $Li_3@B_{40}$ and $Li_3@C_{60}$ systems at BP86-D3/def2-TZVPPD//BP86-D3/def2-TZVPP level.

Systems	CP	Type	$\rho(r_c)$	$\nabla^2\rho(r_c)$	$G(r_c)$	$V(r_c)$	$H(r_c)$	N(pop)	LI	%LI
$Li_3@B_{40}$	NNA	(3,–3)	0.016	–0.015	0.001	–0.006	–0.005	0.17	0.02	12
	NNA–Li	(3,–1)	0.015	–0.004	0.003	–0.008	–0.005			
$Li_3@C_{60}$	NNA	(3,–3)	0.018	–0.018	0.000	–0.005	–0.005	0.59	0.27	46
	NNA–Li	(3,–1)	0.015	0.004	0.005	–0.008	–0.004			

system, a greater extent of charge transfer takes place from Li_3 to B_{40} cage as predicted by the greater positive charges on Li atoms for this system. It is reported that for $La@C_{82}$ system 3 $|e|$ transferred from the La atom to the C_{82} cage (Bethune et al., 1993). Again, in $Sc_3N@C_{80}$ system charge transfer occurs from Sc_3N fragment to C_{80} cage by 6 $|e|$ unit (Iiduka et al., 2005). But for $F_2@C_{60}$ system the charge transfer occurs in a reverse way i.e. from C_{60} cage to F_2 molecule (Foroutan-Nejad et al., 2018).

Atoms in Molecule Analysis

The electron density descriptors of both these systems have been computed at relevant bond critical points (BCPs) and the numerical values are given in **Table 1**. We have also generated the corresponding molecular graphs for these systems and are presented in **Figure 7**. From this analysis, it is confirmed that a non-nuclear attractor (NNA) [(3, –3) type of bond critical point] is present at the center of the Li_3 cluster for both these systems. The negative values of Laplacian of electron density [$\nabla^2\rho(r_c)$] at both the NNAs indicate the electron localization therein. We have found that both $Li_3@B_{40}$ and $Li_3@C_{60}$ systems contained three NNA-Li bond paths which are (3,-1) type of bond critical points. The contour plots of $\nabla^2\rho(r)$ for both systems are presented in **Figure 8A**, which indicates a portion of the electron localization at the center of the Li_3 cluster. The NNA populations are 0.17 $|e|$ and 0.59 $|e|$ with 12% and 46% localization of electron density for $Li_3@B_{40}$ and $Li_3@C_{60}$ systems, respectively. The population of NNA and the percentage localization of electron density at the NNA for $Li_3@C_{60}$ system is higher than that of the $Li_3@B_{40}$ system. The electron-deficient nature of boron (B) atoms may cause the lowering of percentage of localization of electron density at the NNA for $Li_3@B_{40}$ system as compared to $Li_3@C_{60}$ system, where such an effect is absent. The B_{40} cage attracts the electron density from the Li_3 cluster more toward itself and hence decreases the electron density at the center of the Li_3 cluster.

We have generated the electron localization function basin (ELF) plots for both the studied systems and are presented in

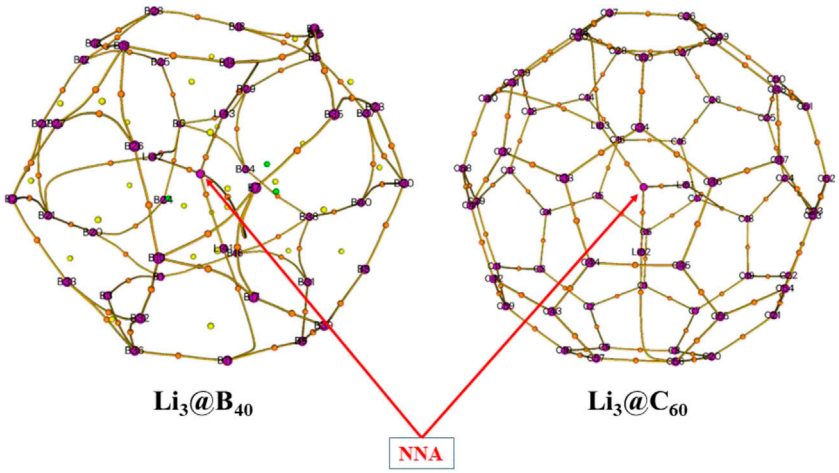

FIGURE 7 | The plots of molecular graphs of $Li_3@B_{40}$ and $Li_3@C_{60}$ systems generated at BP86-D3/def2-TZVPPD//BP86-D3/def2-TZVPP level.

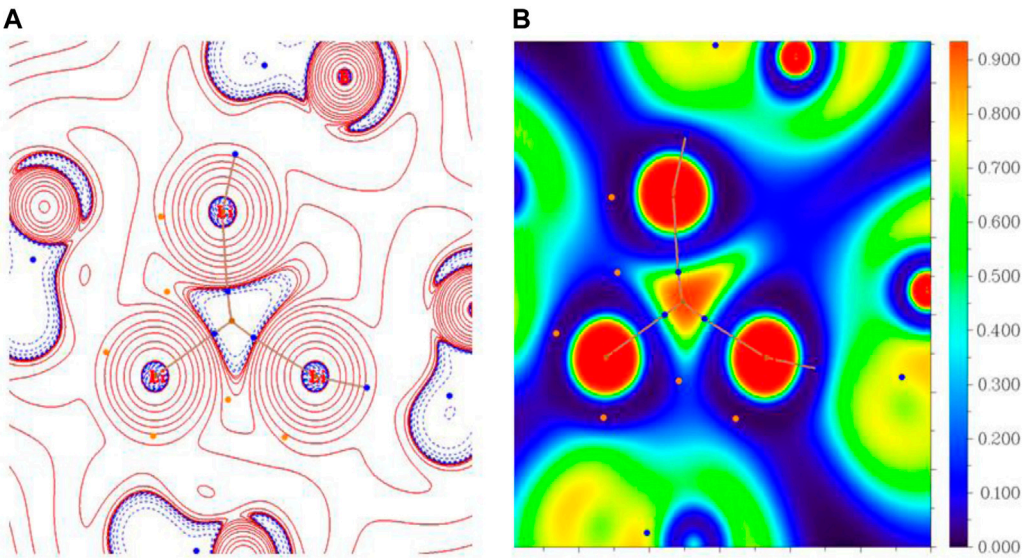

FIGURE 8 | The plots of **(A)** the Laplacian of electron density [$\nabla^2\rho(r)$], blue dashed and red solid lines indicate $\nabla^2\rho(r) < 0$ and $\nabla^2\rho(r) > 0$ regions, respectively; **(B)** the electron localization function (ELF) basin of $Li_3@B_{40}$ and $Li_3@C_{60}$ systems.

Figure 8B. From the plot, it is shown that a basin is present at the center of the Li_3 cluster for both systems. The basin population is 0.58 $|e|$ with 22% localization of electron density for the $Li_3@B_{40}$ system. However, for the $Li_3@C_{60}$ system, the population of the basin is 1.01 $|e|$ with 56% localization of electron density. The ELF basin population of the $Li_3@C_{60}$ system is higher than that of the $Li_3@B_{40}$ system. The lowering of the basin population for the $Li_3@B_{40}$ system is due to the electron-deficient nature of boron (B) atoms. From these results, it can be said that a portion of electron density is localized at the center of the Li_3 cluster in both the systems. The higher values of NNA and ELF populations at the center of the Li_3 cluster of $Li_3@C_{60}$ system as compared to the $Li_3@B_{40}$ system indicates a greater extent of localization of electron density in the $Li_3@C_{60}$ system.

TABLE 2 | Average linear polarizability ($\bar{\alpha}$), first hyperpolarizability (β), and second hyperpolarizability ($\gamma_{\parallel}$) of $Li_3@B_{40}$ and $Li_3@C_{60}$ systems.

NLO property	$Li_3@B_{40}$	$Li_3@C_{60}$
$\bar{\alpha}$	554.2	584.7
β	129.4	79.9
$\gamma_{\parallel}$	3.6×10^5	2.1×10^5

Nonlinear Optical Property

As electride materials contain loosely bound excess electrons, they showed high values of NLO properties. For this purpose, we have computed average polarizability ($\overline{\alpha}$), first hyperpolarizability (β), and second hyperpolarizability ($\gamma_{\parallel}$) for both the systems, and the numerical values are given in **Table 2**. Among both these systems $Li_3@C_{60}$ system shows higher values of $\overline{\alpha}$ and the $Li_3@B_{40}$ system shows higher values of β and$\gamma_{\parallel}$. We have compared the NLO values of our systems with some previously reported known electride materials, for example, M@calix (M = Li, Na; calix = calix [4]pyrrole), $Li@B_{10}H_{14}$ (Muhammad et al., 2011), and M_2 (TCNQ) (Li et al., 2008) (M = Li, Na; TCNQ = Tetracyanoquinodimethane) and are presented in **Supplementary Table S2**. Our systems show comparatively higher values of $\overline{\alpha}$ but lower values of β than the systems under comparison. The numerical values of $\gamma_{\parallel}$ of our systems are comparable with that of the systems being compared.

Electride Properties

It has been observed that in both the systems an NNA is present in the middle of the Li_3 cluster. An ELF basin has appeared in the position where the NNA is present and the values of $\nabla^2\rho$ are negative therein. Both the systems under study exhibit high values of NLO properties. All the criteria for an electride material have been satisfied by these systems. So, $Li_3@B_{40}$ and $Li_3@C_{60}$ systems can be classified as electrides. $Li_3@C_{60}$ system will show better electride characteristics than the $Li_3@B_{40}$ system.

SUMMARY AND CONCLUSION

The stability of $Li_3@B_{40}$ and $Li_3@C_{60}$ systems has been studied using density functional theory (DFT) based computations. The thermochemical results show the spontaneous formation of both the systems as predicted by the negative values of Gibbs' free energy change (ΔG). Due to the confinement, the Li-Li bonds in both the systems are shorter than that in the free Li_3 cluster and the Li-Li vibrational frequencies are increased on confinement. The Li-Li bonds are shorter in the $Li_3@B_{40}$ system as compared to that in the $Li_3@C_{60}$ system. The numerical values of Li-Li bond vibrational frequencies in the $Li_3@B_{40}$ system are higher than that in the $Li_3@C_{60}$ system. The results from the ADMP simulation showed that the systems are stable both at room temperature (300 K) and at 500 K temperature and 1 atm pressure. So, the host B_{40} and C_{60} cages can take the Li_3 cluster inside their cavity and stabilize the cluster. The topological analysis of electron density shows the presence of an NNA at the center of the Li_3 cluster of both these systems and a portion of electron density gets localized therein. The Laplacian of electron density is negative at the NNAs. $Li_3@C_{60}$ system has higher values of NNA and ELF population than that of $Li_3@B_{40}$ system. Our designed endohedral $Li_3@B_{40}$ and $Li_3@C_{60}$ systems behave as electride. $Li_3@C_{60}$ system shows better electride characteristics than $Li_3@B_{40}$ system. As the systems under study behave as electrides, they have the potential to show catalytic activity.

DATA AVAILABILITY STATEMENT

The original contributions presented in the study are included in the article/**Supplementary Material**, further inquiries can be directed to the corresponding author.

AUTHOR CONTRIBUTIONS

PD designed the complex systems under study and executed the computational work. He prepared the first draft of the manuscript. PKC supervised the complete work and critically scrutinized the manuscript.

ACKNOWLEDGMENTS

PKC thanks the topic editors, Professors Soumyajit Roy, Sailaja Krishnamurty and Wolfgang Schöfberger for inviting him to contribute to this special issue honoring Professor Sourav Pal on his sixty-fifth birth anniversary. He would also like to thank DST, New Delhi, India for the J. C. Bose National Fellowship, grant number SR/S2/JCB-09/2009. PD thanks to UGC, New Delhi, India for the Research Fellowship.

SUPPLEMENTARY MATERIAL

The Supplementary Material for this article can be found online at: https://www.frontiersin.org/articles/10.3389/fchem.2021.638581/full#supplementary-material.

REFERENCES

Andreoni, W., and Curioni, A. (1996). Freedom and constraints of a metal atom encapsulated in fullerene cages. *Phys. Rev. Lett.* 77, 834. doi:10.1103/PhysRevLett.77.834

Bader, R. F. W. (1990). *Atoms in molecules. A quantum theory*. Oxford, United Kingdom: Oxford University Press

Becke, A. D. (1988). Density-functional exchange-energy approximation with correct asymptotic behavior. *Phys. Rev. A.* 38, 3098. doi:10.1103/PhysRevA.38.3098

Bethune, D. S., Johnson, R. D., Salem, J. R., de Vries, M. S., and Yannoni, C. S. (1993). Atoms in carbon cages: the structure and properties of endohedral fullerenes. *Nature* 366, 123–128. doi:10.1038/366123a0

Bishop, D. M., and Norman, P. (2001). *Handbook of advanced electronic and photonic materials*; Editor H. S. Nalwas, San Diego, CA: Academic, Vol. 9, 1–240(.)

Bloodworth, S., Sitinova, G., Alom, S., Vidal, S., Bacanu, G. R., Elliott, S. J., et al. (2019). First synthesis and characterization of $CH_4@C_{60}$. *Angew. Chem. Int. Ed.* 58, 5038–5043. doi:10.1002/anie.201900983

Buchammagari, H., Toda, Y., Hirano, M., Hosono, H., Takeuchi, D., and Osakada, K. (2007). Room temperature-stable electride as a synthetic organic reagent: application to pinacol coupling reaction in aqueous media. *Org. Lett.* 9, 4287–4289. doi:10.1021/ol701885p

Bühl, M., Patchkovskii, S., and Thiel, W. (1997). Interaction energies and NMR chemical shifts of noble gases in C_{60}. *Chem. Phys. Lett.* 275, 14–18. doi:10.1016/s0009-2614(97)00733-1

Cagle, D. W., Thrash, T. P., Alford, M., Chibante, L. P. F., Ehrhardt, G. J., and Wilson, L. J. (1996). Synthesis, characterization, and neutron activation of holmium. *Metallofullerenes. J. Am. Chem. Soc.* 118, 8043–8047. doi:10.1021/ja960841z

Chakraborty, D., Pan, S., and Chattaraj, P. K. (2016). Encapsulation of small gas molecules and rare gas atoms inside the octa acid cavitand. *Theor. Chem. Acc.* 135, 119. doi:10.1007/s00214-016-1876-y

Chen, Q., Li, W-L., Zhao, Y-F., Zhang, S-Y., Hu, H-S., Bai, H., et al. (2015). Experimental and theoretical evidence of an axially chiral borospherene. *ACS Nano* 9, 754–760. doi:10.1021/nn506262c

Choi, S., Kim, Y. J., Kim, S. M., Yang, J. W., Kim, S. W., and Cho, E. J. (2014). Hydrotrifluoromethylation and iodotrifluoromethylation of alkenes and alkynes using an inorganic electride as a radical generator. *Nat. Commun.* 5, 1038–1046. doi:10.1038/ncomms5881

Dale, S. G., and Johnson, E. R. (2018). Theoretical descriptors of electrides. *J. Phys. Chem. A.* 122, 9371–9391. doi:10.1021/acs.jpca.8b08548

Dale, S. G., Otero-de-la-Roza, A., and Johnson, E. R. (2014). Density-functional description of electrides. *Phys. Chem. Chem. Phys.* 16, 14584–14593. doi:10.1039/C3CP55533J

Das, P., and Chattaraj, P. K. (2020). Electride characteristics of some binuclear sandwich complexes of alkaline earth metals, $M_2(\eta^5\text{-}L)_2$ (M = Be, Mg; L = $C_5H_5^-$, N_5^-, P_5^-, As_5^-). *J. Phys. Chem. A.* 124, 9801−9810. doi:10.1021/acs.jpca.0c08306

Das, P., Saha, R., and Chattaraj, P. K. (2020). Encapsulation of Mg_2 inside a C_{60} cage forms an electride. *J. Comput.Chem.* 31, 1645–1653. doi:10.1002/jcc.26207

Das, R., and Chattaraj, P. K. (2014). Guest–host interaction in an aza crown analog. *Int. J. Quan. Chem.* 114, 708–719. doi:10.1002/qua.24648

Ding, J., and Yang, S. (1996). Isolation and characterization of Pr@C_{82} and Pr_2@C_{80}. *J. Am. Chem. Soc.* 118, 11254–11257. doi:10.1021/ja961601m

Dye, J. L., DeBacker, M. G., and Dorfman, L. M. (1970). Pulse radiolysis studies. XVIII. Spectrum of the solvated electron in the systems ethylenediamine–water and ammonia–water. *J. Chem. Phys.* 52, 6251–6258. doi:10.1063/1.1672935

Dye, J. L. (1991). Electrides and alkalides-comparison with metal solutions. *J. Phys. IV.* 1, 259–282. doi:10.1051/jp4:1991531

Dye, J. L. (1997). Electrides: from 1D heisenberg chains to 2D pseudo-metals. *Inorg. Chem.* 36, 3816–3826. doi:10.1021/ic970551z

Dye, J. L. (1990). Electrides: ionic salts with electrons as the anions. *Science* 247, 663–668. doi:10.1126/science.247.4943.663

Dye, J. L. (2003). Electrons as anions. *Science* 301, 607–608. doi:10.1126/science.1088103

Ellaboudy, A., Dye, J. L., and Smith, P. B. (1983). Cesium 18-crown-6 compounds. A crystalline ceside and a crystalline electride. *J. Am.Chem. Soc.* 105, 6490–6491. doi:10.1021/ja00359a022

Foroutan-Nejad, C., Straka, M., Fernàndez, I., and Frenking, G. (2018). Buckyball difluoride F_2^-@C_{60}^+—a single-molecule crystal. *Angew. Chem. Int. Ed.* 57, 13931–13934. doi:10.1002/anie.201809699

Frisch, M. J., Trucks, G. W., Schlegel, H. B., Scuseria, G. E., Robb, M. A., Cheeseman, J. R., et al. (2016). *Gaussian 16, Revision B.01*. Wallingford, CT: Gaussian, Inc.

Garcia-Borràs, M., Solà, M., Luis, J. M., and Kirtman, B. (2012). Electronic and vibrational nonlinear optical properties of five representative electrides. *J. Chem. Theor. Comput.* 8, 2688–2697. doi:10.1021/ct300433q

Glendening, E. D., Reed, A. E., Carpenter, J. E., and Weinhold, F. (1990). *NBO 3.1 QCPE bulletin*, 10, 58

Greenlee, K. W., and Henne, A. L. (1946). Sodium amide. *Inorg. Synth.* 2, 128–135. doi:10.1002/9780470132333.ch38

Grimme, S., Antony, J., Ehrlich, S., and Krieg, H. (2010). A consistent and accurate ab initio parametrization of density functional dispersion correction (DFT-D) for the 94 elements H-Pu. *J. Chem. Phys.* 132, 154104. doi:10.1063/1.3382344

Heath, J. R., O'Brien, S. C., Zhang, Q., Liu, Y., Curl, R. F., Tittel, F. K., et al. (1985). Lanthanum complexes of spheroidal carbon shells. *J. Am. Chem. Soc.* 107, 7779–7780. doi:10.1021/ja00311a102

Huang, R. H., Wagner, M. J., Gilbert, D. J., Reidy-Cedergren, K. A., Ward, D. L., Faber, M. K., et al. (1997). Structure and properties of Li^+(cryptand [2.1.1])e^-, an electride with a 1D "spin-ladder-like" cavity-channel geometry. *J. Am. Chem. Soc.* 119, 3765–3772. doi:10.1021/ja9640760

Iiduka, Y., Ikenaga, O., Sakuraba, A., Wakahara, T., Tsuchiya, T., Maeda, Y., et al. (2005). Chemical reactivity of Sc_3N@C_{80} and La_2@C_{80}. *J. Am. Chem. Soc.* 127, 9956–9957. doi:10.1021/ja052534b

Jaroš, A., Bonab, E. F., Straka, M., and Foroutan-Nejad, C. (2019). Fullerene-based switching molecular diodes controlled by oriented external electric fields. J. Am. Chem. Soc. 141, 19644–19654. doi:10.1021/jacs.9b07215

Kato, H., Asakura, K., and Kudo, A. (2003). Highly efficient water splitting into H_2 and O_2 over lanthanum-doped $NaTaO_3$ photocatalysts with high crystallinity and surface nanostructure. *J. Am. Chem. Soc.* 125, 3082–3089. doi:10.1021/ja027751g

Khatua, M., Pan, S., and Chattaraj, P. K. (2014a). Confinement of $(HF)_2$ in C_n(n = 60, 70, 80, 90) cages. *Chem. Phys. Lett.* 616–617, 49–54. doi:10.1016/j.cplett.2014.10.025

Khatua, M., Pan, S., and Chattaraj, P. K. (2014b). Movement of Ng_2 molecules confined in a C_{60} cage: an ab initio molecular dynamics study. *Chem. Phys. Lett.* 610–611, 351–356. doi:10.1016/j.cplett.2014.06.052

Kim, Y. J., Kim, S. M., Hosono, H., Yang, J. W., and Kim, S. W. (2014). The scalable pinacol coupling reaction utilizing the inorganic electride $[Ca_2N]^+\cdot e^-$ as an electron donor. *Chem. Comm.* 50, 4791–4794. doi:10.1039/C4CC00802B

Kitano, M., Inoue, Y., Yamazaki, Y., Hayashi, F., Kanbara, S., Matsuishi, S., et al. (2012). Ammonia synthesis using a stable electride as an electron donor and reversible hydrogen store. *Nat. Chem.* 4, 934–940. doi:10.1038/nchem.1476

Kitano, M., Kanbara, S., Inoue, Y., Kuganathan, N., Sushko, P. V., Yokoyama, T., et al. (2015). Electride support boosts nitrogen dissociation over ruthenium catalyst and shifts the bottleneck in ammonia synthesis. *Nat. Commum.* 6, 6731–6739. doi:10.1038/ncomms7731

Komatsu, K., Murata, M., and Murata, Y. (2005). Encapsulation of molecular hydrogen in fullerene C_{60} by organic synthesis. *Science* 307, 238–240. doi:10.1126/science.1106185

Krachmalnicoff, A., Bounds, R., Mamone, S., Alom, S., Concistrè, M., Meier, B., et al. (2016). The dipolar endofullerene HF@C_{60}. *Nat. Chem* 8, 953–957. doi:10.1038/nchem.2563

Krapp, A., and Frenking, G. (2007). Is this a chemical bond? A theoretical study of Ng_2@C_{60} (Ng=He, Ne, Ar, Kr, Xe). *Chem. Eur. J.* 13, 8256–8270. doi:10.1002/chem.200700467

Kroto, H. W., Heath, J. R., Obrien, S. C., Curl, R. F., and Smalley, R. E. (1985). C60: buckminsterfullerene. *Nature* 318, 162–163. doi:10.1038/318162a0

Kubozono, Y., Maeda, H., Takabayashi, Y., Hiraoka, K., Nakai, T., Kashino, S., et al. (1996). Extractions of Y@C_{60}, Ba@C_{60}, La@C_{60}, Ce@C_{60}, Pr@C_{60}, Nd@C_{60}, and Gd@C_{60} with aniline. *J. Am. Chem. Soc.* 118, 6998–6999. doi:10.1021/ja9612460

Kurotobi, K., and Murata, Y. (2011). A single molecule of water encapsulated in fullerene C_{60}. *Science* 333, 613–616. doi:10.1126/science.1206376

Lee, K., Kim, S. W., Toda, Y., Matsuishi, S., and Hosono, H. (2013). Dicalcium nitride as a two-dimensional electride with an anionic electron layer. *Nature* 494, 336–340. doi:10.1038/nature11812

Levitt, M. H. (2013). Spectroscopy of light-molecule endofullerenes. *Phil Trans. R. Soc. A.* 371, 20120429. doi:10.1098/rsta.2012.0429

Li, H-R., Chen, Q., Tian, X-X., Lu, H-G., Zhai, H-J., and Li, S-D. (2016a). Cage-like B_{40}^+: a perfect borospherene monocation. *J. Mol. Model.* 22, 124. doi:10.1007/s00894-016-2980-6

Li, H. R., Jian, T., Li, W. L., Miao, C. Q., Wang, Y. J., Chen, Q., et al. (2016). Competition between quasi-planar and cage-like structures in the B_{29}^- cluster: photoelectron spectroscopy and ab initio calculations. *Phys. Chem. Chem. Phys.* 18, 29147–29155. doi:10.1039/C6CP05420J

Li, S., Zhang, Z., Long, Z., and Qin, S. (2017). Structures, stabilities and spectral properties of borospherene B_{44}^- and metalloborospherenes $MB_{44}^{0/-}$ (M = Li, Na, and K). *Sci. Rep.* 7, 40081. doi:10.1038/srep40081

Li, Z.-J., Wang, F.-F., Li, Z.-R., Xu, H.-L., Huang, X.-R., Wu, D., et al. (2008). Large static first and second hyperpolarizabilities dominated by excess electron transition for radical ion pair salts $M_2^{\cdot+}TCNQ^{\cdot-}$ (M = Li, Na, K). *Phys. Chem. Chem. Phys.* 11, 402. doi:10.1039/b809161g

Lu, T., and Chen, F. (2012). Multiwfn: a multifunctional wavefunction analyzer. *J. Comput. Chem.* 33, 580–592. doi:10.1002/jcc.22885

Lu, Y., Li, J., Tada, T., Toda, Y., Ueda, S., Yokoyama, T., et al. (2016). Water durable electride Y_5Si_3: electronic structure and catalytic activity for ammonia synthesis. *J. Am. Chem. Soc.* 138, 3970–3973. doi:10.1021/jacs.6b00124

Lv, J., Wang, Y., Zhu, L., and Ma, Y. (2014). B38: an all-boron fullerene analogue. *Nanoscale* 6, 11692–11696. doi:10.1039/C4NR01846J

Marqués, M., Ackland, G. J., Lundegaard, L. F., Stinton, G., Nelmes, R. J., McMahon, M. I., et al. (2009). Potassium under pressure: a pseudobinary

ionic compound. *J. Phys. Rev. Lett.* 103, 115501. doi:10.1103/PhysRevLett.103.115501

Matsuishi, S., Toda, Y., Miyakawa, M., Hayashi, K., Kamiya, T., Hirano, M., et al. (2003). High-density electron anions in a nanoporous single crystal: $[Ca_{24}Al_{28}O_{64}]^{4+}(4e^-)$. *Science* 301, 626–629. doi:10.1126/science.1083842

Mei, C., Edgecombe, K. E., Smith, V. H., and Heilingbrunner, A. (1993). Topological analysis of the charge density of solids: bcc sodium and lithium. *International Journal Quantum Chemistry* 48, 287–293. doi:10.1002/qua.560480503

Miyakawa, M., Kim, S. W., Hirano, M., Kohama, Y., Kawaji, H., Atake, T., et al. (2007). Superconductivity in an inorganic electride $12CaO{\cdot}7Al_2O_3{:}e^-$. *J. Am. Chem. Soc.* 129, 7270–7271. doi:10.1021/ja0724644

Muhammad, S., Xu, H., and Su, Z. (2011). Capturing a synergistic effect of a conical push and an inward pull in fluoro derivatives of $Li@B_{10}H_{14}$ basket: toward a higher vertical ionization potential and nonlinear optical response. *J. Phys. Chem. A.* 115, 923–931. doi:10.1021/jp110401f

Murata, M., Maeda, S., Morinaka, Y., Murata, Y., and Komatsu, K. (2008). Synthesis and reaction of fullerene C70 encapsulating two molecules of H2. *J. Am. Chem. Soc.* 130, 15800–15801. doi:10.1021/ja8076846.Ohtsuki

Ohtsuki, T., Ohno, K., Shiga, K., Kawazoe, Y., Maruyama, Y., and Masumoto, K. (1998). Insertion of Xe and Kr atoms into C_{60} and C_{70} fullerenes and the formation of dimers. *Phys. Rev. Lett.* 81, 967. doi:10.1103/PhysRevLett.81.967

Okada, H., Komuro, T., Sakai, T., Matsuo, Y., Ono, Y., Omote, K., et al. (2012). Preparation of endohedral fullerene containing lithium ($Li@C_{60}$) and isolation as pure hexafluorophosphate salt ($[Li^+@C_{60}][PF_6^-]$). *RSC Adv.* 2, 10624–10631. doi:10.1039/C2RA21244G

Pan, S., Ghara, M., Kar, S., Zarate, X., Merino, G., and Chattaraj, P. K. (2018). Noble gas encapsulated B_{40} cage. *Phys. Chem. Chem. Phys.* 20, 1953–1963. doi:10.1039/C7CP07890K

Pan, S., Mandal, S., and Chattaraj, P. K. (2015). Cucurbit[6]uril: a possible host for noble gas atoms. *J. Phys. Chem. B.* 119, 10962–10974. doi:10.1021/acs.jpcb.5b01396

Perdew, J. P. (1986). Density-functional approximation for the correlation energy of the inhomogeneous electron gas. *Phys. Rev. B.* 33, 8822. doi:10.1103/PhysRevB.33.8822

Postils, V., Garcia-Borràs, M., Solà, M., Luis, J. M., and Matito, E. (2015). On the existence and characterization of molecular electrides. *Chem. Commun.* 51, 4865–4868. doi:10.1039/C5CC00215J

Redko, M. Y., Jackson, J. E., Huang, R. H., and Dye, J. L. (2005). Design and synthesis of a thermally stable organic electride. *J. Am. Chem. Soc.* 127, 12416–12422. doi:10.1021/ja053216f

Reed, A. E., Curtiss, L. A., and Weinhold, F. (1988). Intermolecular interactions from a natural bond orbital, donor-acceptor viewpoint. *Chem. Rev.* 88, 899–926. doi:10.1021/cr00088a005

Saha, R., Das, P., and Chattaraj, P. K. (2019). A complex containing four magnesium atoms and two Mg–Mg bonds behaving as an electride. *Eur. J. Inorg. Chem.* 2019 (38), 4105–4111. doi:10.1002/ejic.201900813

Saunders, M., Jimenez-Vazquez, H. A., Cross, R. J., Mroczkowski, S., Gross, M. L., Giblin, D. E., et al. (1994). Incorporation of helium, neon, argon, krypton, and xenon into fullerenes using high pressure. *J. Am. Chem. Soc.* 116, 2193–2194. doi:10.1021/ja00084a089

Saunders, M., Jiménez-Vázquez, H. A., Cross, R. J., and Poreda, R. J. (1993). Stable compounds of helium and neon: $He@C_{60}$ and $Ne@C_{60}$. *Science* 259, 1428–1430. doi:10.1126/science.259.5100.1428

Singh, D. J., Krakauer, H., Haas, C., and Pickett, W. E. (1993). Theoretical determination that electrons act as anions in the electride Cs^+ (15-crown-5)$_2{\cdot}e^-$. *Nature* 365, 39–42. doi:10.1038/365039a0

Strenalyuk, T., and Haaland, A. (2008). Chemical bonding in the inclusion complex of He in adamantane (He@Adam): the origin of the barrier to dissociation. *Chem. Eur. J.* 14, 10223–10226. doi:10.1002/chem.200800715

Sun, W. -M., Li, X. -H., Li, Y., Ni, B. -L., Chen, J. -H., Li, C. -Y., et al. (2016). Theoretical study of the substituent effects on the nonlinear optical properties of a room-temperature- stable organic electride. *Chem. Phys. Chem.* 17, 3907–3915. doi:10.1002/cphc.201600970

Tai, T. B., and Nguyen, M. T. (2016). A new chiral boron cluster B44 containing nonagonal holes. *Chem. Commun.* 52, 1653–1656. doi:10.1039/C5CC09111J

Tai, T. B., and Nguyen, M. T. (2017). Aromatic cage-like B_{46}: existence of the largest decagonal holes in stable atomic clusters. *RSC Adv.* 7, 22243–22247. doi:10.1039/C7RA02870A

Tian, W. J., Chen, Q., Li, H. R., Yan, M., Mu, Y. W., Lu, H. G., et al. (2016). Saturn-like charge- transfer complexes $Li_4\&B_{36}$, $Li_5\&B_{36}^+$, and $Li_6\&B_{36}^{2+}$: exohedral metalloborospherenes with a perfect cage-like B_{36}^{4-} core. *Phys. Chem. Chem. Phys.* 18, 9922–9926. doi:10.1039/C6CP01279E

Toda, Y., Hirayama, H., Kuganathan, N., Torrisi, A., Sushko, P. V., and Hosono, H. (2013). Activation and splitting of carbon dioxide on the surface of an inorganic electride material. *Nat. Commun.* 4, 2378–2385. doi:10.1038/ncomms3378

Ueno, H., Nishihara, T., Segawa, Y., and Itami, K. (2015). Cycloparaphenylene-based ionic donor–acceptor supramolecule: isolation and characterization of $Li^+@C_{60}\subset$[10]CPP. *Angew. Chem. Int. Ed.* 54, 3707. doi:10.1002/anie.201500544

Wagner, M. J., Huang, R. H., Eglin, J. L., and Dye, J. L. (1994). An electride with a large six-electron ring. *Nature*. 368, 726–729. doi:10.1038/368726a0

Wan, S. M., Zhang, H. –W., Nakane, T., Xu, Z., Inakuma, M., Shinohara, H., et al. (1998). Production, isolation, and electronic properties of missing Fullerenes: $Ca@C_{72}$ and $Ca@C_{74}$. *J. Am. Chem. Soc.* 120, 6806–6807. doi:10.1021/ja972478h

Ward, D. L., Huang, R. H., and Dye, J. L. (1988). Structures of alkalides and electrides. I. Structure of potassium cryptand[2.2.2] electride. *Acta Crystallogr. Sect. C: Cryst. Struct. Commun.* 44, 1374–1376. doi:10.1107/S0108270188002847

Ward, D. L., Huang, R. H., and Dye, J. L. (1990a). The structures of alkalides and electrides. III. Structure of potassium cryptand[2.2.2] natride. *Acta Crystallogr. Sect. C: Cryst. Struct. Commun.* 46, 1833–1835. doi:10.1107/S0108270190001007

Ward, D. L., Huang, R. H., and Dye, J. L. (1990b). The structures of alkalides and electrides. V. Structures of caesium bis (15-crown-5) kalide and rubidium bis (15-crown-5) rubidide. *Acta Crystallogr. Sect. C: Cryst. Struct. Commun.* 46, 1838–1841. doi:10.1107/S0108270190002293

Weigend, F., and Ahlrichs, R. (2005). Balanced basis sets of split valence, triple zeta valence and quadruple zeta valence quality for H to Rn: design and assessment of accuracy. *Phys. Chem. Chem. Phys.* 7, 3297–3305. doi:10.1039/B508541A

Xie, Q., Huang, R. H., Ichimura, A. S., Phillips, R. C., Pratt, W. P., and Dye, J. L. (2000). Structure and properties of a new electride, Rb^+(cryptand- [2.2.2])e^-. *J. Am. Chem. Soc.* 122, 6971–6978. doi:10.1021/ja9943445

Yanagi, H., Kim, K.-B., Koizumi, I., Kikuchi, M., Hiramatsu, H., Miyakawa, M., et al. (2009). Low Threshold Voltage and Carrier Injection Properties of Inverted Organic Light-Emitting Diodes with $[Ca_{24}Al_{28}O_{64}]^{4+}(4e^-)$ Cathode and $Cu_{2-x}Se$ Anode. *J. Phys. Chem. C.* 113, 18379–18384. doi:10.1021/jp906386q

Zhai, H-J., Zhao, Y-F., Li, W-L., Chen, Q., Bai, H., Hu, H-S., et al. (2014). Observation of an all- boron fullerene. *Nat. Chem.* 6, 727–731. doi:10.1038/nchem.1999

Zhao, J., Huang, X., Shi, R., Liu, H., Sua, Y., and King, R. B. (2015). B_{28}: the smallest all- boron cage from an ab initio global search. *Nanoscale* 7, 15086–15090. doi:10.1039/C5NR04034E

Zhao, S., Kan, E., and Li, Z. (2016). Electride: from computational characterization to theoretical design. *Wires Comput. Mol. Sci.* 6, 430–440. doi:10.1002/wcms.1258

Zurek, E., Edwards, P. P., and Hoffmann, R. (2009). A molecular perspective on lithium- ammonia solutions. *Angew. Chem. Int. Ed.* 48, 8198–8232. doi:10.1002/anie.200900373

Conflict of Interest: The authors declare that the research was conducted in the absence of any commercial or financial relationships that could be construed as a potential conflict of interest.